Vietnam Journal of Catalysis and Adsorption
Tạp chí xúc tác và hấp phụ Việt Nam

https://jca.edu.vn

Removal of polystyrene (PS) microplastics using a magnetic Fe_3O_4@MIL-101(Cr) composite

Pham Xuan Nui[1,*], Phan Thi Huong Phu[1], Nguyen Thi Hang[2], Le Dinh Khiem[3], Nguyen Thi Phuong Lan[4]

[1]*Deparment of Chemical Engineering, Hanoi University of Mining and Geology, 18-Vien Street, Dong Ngac Ward, Hanoi, Vietnam.*
[2] *University of Transport Ho Chi Minh City, No. 2 Vo Oanh Street, Thanh My Tay Ward, Ho Chi Minh City, Vietnam.*
[3] *Chemistry–Materials Research Laboratory, Institute of Air Defense–Air Force Engineering, 166 Hoang Van Thai Street, Phuong Liet Ward, Hanoi, Vietnam.*
[4] *Faculty of Basic Sciences, University of Economics–Technology for Industries, No. 456 Minh Khai Street, Vinh Tuy Ward, Hanoi, Vietnam.*
** E-mail: phamxuannui@humg.edu.vn*

ARTICLE INFO

Received: 16/03/2026
Accepted: 12/04/2026
Published: 30/06/2024

Keywords:
Fe_3O_4@MIL-101(Cr) composite; polystyrene (PS); microplastics (MPs); removal of PSMPs.

ABSTRACT

In this study, a Fe_3O_4@MIL-101(Cr) composite material was synthesized through a simple approach combining Fe_3O_4 and MIL-101(Cr), using waste PET as the raw material source. The obtained composite exhibited magnetic properties with a saturation magnetization of approximately 18 emu g^{-1}, compared with 50 emu g^{-1} for pure Fe_3O_4. The synthesized materials were then employed as adsorbents for the removal of polystyrene (PS) microplastics from aqueous environments. The experimental results showed that under optimal conditions (pH = 8.15, room temperature, and an adsorbent dosage of Fe_3O_4@MIL-101(Cr) of 1.25 g L^{-1}), the removal efficiency of PS reached approximately 91.4 ± 3.74% after 150 min of interaction. Furthermore, the Fe_3O_4@MIL-101(Cr) composite could be easily recovered using an external magnetic field, demonstrating its potential as an environmentally friendly and recyclable adsorbent for the treatment of microplastic contamination in aquatic environments.

Introduction

Plastic production has increased significantly in recent decades, reaching approximately 0.3 billion tons per year, of which about half is intended for single-use applications [1, 2]. Microplastics occur in a wide range of sizes and shapes with diverse chemical compositions, including aliphatic or aromatic hydrocarbon structures. Microplastic particles present in soil can also be transported through river and stream flows and eventually reach the marine environment [3-5]. In addition to industrial and manufacturing activities, the direct disposal of single-use plastics, washing of synthetic textiles, microbeads from cosmetic products, tire wear particles, and the fragmentation of larger plastic debris are major sources contributing to the introduction of microplastics into aquatic systems [6].

Currently, various technologies have been developed for the removal of microplastics, including physical,

https://doi.org/10.62239/jca.2026.017
6

©2026 by the authors. Licensee Vietnam Journal of Catalysis and Adsorption. This article is an open access article distributed under the terms and conditions of the Creative Commons Attribution (CC BY) license (https://creativecommons.org/licenses/by/4.0/).

chemical, and biological methods. Biodegradation technologies and bioreactor systems have also been investigated; however, their degradation efficiency remains relatively low and requires long processing times, raising concerns regarding their practical effectiveness and environmental impacts [7-11]. Recently, emerging approaches based on adsorbent materials such as metal–organic frameworks (MOFs) have been proposed for the removal of microplastics from aquatic environments [12]. MOFs can be tailored for specific applications by modifying their composition and pore size, enabling the selective capture of different sizes and types of microplastics. This selectivity allows for more efficient removal of microplastics while minimizing interference with other components in water. Moreover, MOFs can selectively adsorb microplastic particles while leaving other substances in the water largely unaffected. They can also be regenerated and reused over multiple cycles, making them more cost-effective and sustainable compared with single-use filtration systems or other methods that require frequent replacement. In addition, MOFs can be synthesized from non-toxic materials (e.g., waste PET bottles) and do not generate harmful byproducts during the purification process, making them a more environmentally friendly option than some conventional methods.

Gnanasekaran *et al.* [13] conducted a study investigating the effectiveness of a MOF-based membrane, MIL-100(Fe), for the removal of microplastics from textile wastewater. MIL-100(Fe) is a MOF containing iron metal ions and terephthalic acid organic ligands, forming a mesoporous structure with a small pore diameter (1.8 nm), a large pore volume (0.8374 cm^3 g^{-1}), and microporous channels that facilitate the transport of small molecules. To fabricate the mixed matrix membrane, hydrophilic MIL-100(Fe) nanoparticles were incorporated into a polysulfone matrix. The incorporation of MIL-100(Fe) significantly influenced the membrane morphology, including its hydrophilicity, adhesion properties, porosity, and pore size distribution. The best performance was achieved with 0.5 wt% MIL-100(Fe) in the polysulfone matrix, resulting in a 10.3-fold increase in pure water flux compared with the pristine polysulfone membrane (M0). The PSF/MIL-100(Fe) membrane exhibited optimal performance under alkaline conditions (pH = 9) due to the electrostatic repulsion mechanism toward cationic contaminants. The study also demonstrated the reusability of the membrane, as the organic ligands within the MIL-100(Fe) structure help maintain structural stability even after several operating cycles.

Mohana *et al.* [14] investigated the behavior of nano-/microplastic particles in wastewater and their removal using membrane processes, particularly focusing on the efficiency of MOF-based membranes in eliminating nano-/microplastics. In their study, a MOF-based UF ED-MIL-101(Cr) membrane was used to remove nano-/microplastic particles from wastewater. Their findings indicated that the UF ED-MIL-101(Cr) membrane exhibited high water permeability and was capable of removing more than 90% of both negatively and positively charged nano-/microplastic particles from wastewater through electrostatic attraction and repulsion mechanisms.

Therefore, MIL-101(Cr) is considered a promising candidate for the adsorption of microplastic particles due to its large specific surface area, high water permeability, and mesoporous structure. In addition, MIL-101(Cr) can be synthesized from waste PET bottles, contributing to the reduction of environmental pollution. Furthermore, incorporating Fe_3O_4 into the adsorbent facilitates the magnetic separation and recovery of the material after the adsorption process. However, to the best of our knowledge, there have been no reports on the use of Fe_3O_4@MIL-101(Cr) composite materials for the removal of microplastics from water via adsorption. Therefore, in this study, a magnetic Fe_3O_4@MIL-101(Cr) composite was synthesized and employed as an adsorbent for the removal of polystyrene (PS) microplastics from aqueous environments.

Experimental

Materials

Terephthalic acid (TPA) recovered from waste PET was obtained following the procedure reported in our previous study [15]. Iron(II) sulfate heptahydrate ($FeSO_4{\cdot}7H_2O$, ≥98%), iron(III) chloride hexahydrate ($FeCl_3{\cdot}6H_2O$, ≥98%), sodium hydroxide (NaOH, ≥98%), ethanol (C_2H_5OH, 96%), chromium(III) nitrate nonahydrate ($Cr(NO_3)_3{\cdot}9H_2O$, 99%), hydrofluoric acid (HF, 40%), dimethylformamide (DMF, 99.8%), ethylene glycol (EG, 99%), hydrochloric acid (HCl, 37%), and potassium chloride (KCl, 99%) were purchased from Sigma-Aldrich. All chemicals were of analytical grade and used as received without further purification.

Synthesis of Fe_3O_4@MIL-101(Cr)

The synthesis of MIL-101(Cr) from PET was carried out according to the procedure reported in our previous study [15]. The magnetic Fe_3O_4 nanoparticles were synthesized as follows: 2.78 g of $FeSO_4{\cdot}7H_2O$ was

https://doi.org/10.62239/jca.2026.017

dissolved in 50 mL of distilled water to obtain solution A. Subsequently, 5.41 g of $FeCl_3 \cdot 6H_2O$ was dissolved in approximately 50 mL of 97% ethanol to form solution B. Solution A was then slowly added to solution B under an inert atmosphere (N_2) for 2 h at a temperature of about 50–60 °C. The pH of the mixture was adjusted to 11 using a NaOH solution. Afterward, the resulting product was allowed to cool, filtered, washed, and dried at 90 °C to obtain dark brown magnetic Fe_3O_4 nanoparticles.

Next, 2 g of the synthesized MIL-101(Cr) was dispersed in 50 mL of an ethanol/water solvent mixture (volume ratio 2:1) to form solution C. Meanwhile, 1.33 g of the obtained Fe_3O_4 nanoparticles was dispersed in 50 mL of ethanol to obtain solution D. Solution C was then slowly added to solution D, followed by ultrasonication for approximately 30 min to ensure homogeneous dispersion. The mixture was subsequently transferred into an autoclave and heated at 120 °C for about 9 h. Finally, the obtained product was filtered, washed with deionized water, and dried at room temperature to obtain the Fe_3O_4@MIL-101(Cr) composite material.

Characterization

The crystalline phase structure of the synthesized materials was analyzed by X-ray diffraction (XRD) using a diffractometer (Bruker, Germany) with Cu Kα radiation (λ = 0.154 nm) at a scanning rate of 0.2° s^{-1}. The surface morphology of the samples was examined using scanning electron microscopy (SEM, Hitachi S-4800-3000F). Fourier transform infrared spectroscopy (FTIR, Jasco 4700) was employed to identify functional groups and bonding characteristics of the synthesized materials before and after microplastic adsorption. The magnetic properties, including the saturation magnetization, were determined using a vibrating sample magnetometer (VSM). The elemental composition was analyzed by energy-dispersive X-ray spectroscopy (EDX) using a JEOL JMS 6490 instrument (Japan).

Removal of PS microplastics using Fe_3O_4@MIL-101(Cr)

The removal of PS microplastics using the Fe_3O_4, MIL-101(Cr) and Fe_3O_4@MIL-101(Cr) composite was carried out as follows. 0.5 g·L^{-1} PS microplastics with an average particle size of approximately 500 nm and 1.5 g·L^{-1} of the material were added to 20 mL of a microplastic suspension. The treatment of the PS microplastics for each material was conducted at a stirring speed of 250 rpm and a temperature of 30 °C for the investigated period. Subsequently, the microplastics were separated from the solution under the attraction of a magnet (magnetic force of approximately ~25 kg).

The separated sample was subsequently dried at 60 °C for approximately 12 h, after which the mass of the adsorbent after adsorption was determined. The removal efficiency of PS microplastics was evaluated using the gravimetric method according to Equation (1).

$$\eta = \frac{(m_2 - m_1)}{m_0} \times 100\% \quad (1)$$

In this equation, m_1 represents the mass of the adsorbent, m_2 denotes the mass of the adsorbent after the adsorption of microplastics, and m_0 is the initial mass of PS microplastics in the solution (m_0 = 25 mg, corresponding to 50 mL of PSMPs with a concentration of 0.5 g L^{-1}).

The average particle size (500 nm) of the microplastics used in the experiment was determined using a laser scattering particle size analyzer (HORIBA LA-960) [16]. All adsorption experiments were performed in triplicate under identical conditions to ensure reproducibility. The experimental data are presented as mean values ± standard deviation (SD). The standard deviation was calculated based on repeated measurements to evaluate the dispersion of the data.

Results and discussion

Characterization of the materials

The results of the XRD pattern (Figure 1(A)) shows that the characteristic diffraction peaks of Fe_3O_4 at 2θ = 30.1°, 35.5°, 43.1°, 53.5°, 57.0°, and 62.6°, corresponding to the (220), (311), (400), (422), (511), and (440) crystal planes of cubic magnetite (JCPDS No. 19-0629) [17]. MIL-101(Cr) exhibits distinct diffraction peaks at low angles (2θ ≈ 5–10°), which are attributed to the ordered porous structure of the MOF framework [15]. In the Fe_3O_4@MIL-101(Cr) composite, the diffraction peaks of both Fe_3O_4 and MIL-101(Cr) are observed, indicating the successful incorporation of magnetic Fe_3O_4 nanoparticles into the MIL-101(Cr) structure without destroying the crystalline framework.

The FT-IR spectrum (Figure 1(B)) of MIL-101(Cr) shows characteristic bands at around 1620 and 1400 cm^{-1}, corresponding to the asymmetric and symmetric stretching vibrations of the carboxylate groups (COO^-) from the terephthalate ligand. A band at approximately 750 cm^{-1} is attributed to the aromatic C–H bending vibration. For Fe_3O_4, the strong absorption band at around 580 cm^{-1} is assigned to the Fe–O stretching vibration of the spinel structure. In the Fe_3O_4@MIL-101(Cr) composite, both the characteristic peaks of Fe_3O_4 and MIL-101(Cr) are observed, indicating the successful incorporation of Fe_3O_4 nanoparticles into the MIL-101(Cr) framework without destroying its structure.

https://doi.org/10.62239/jca.2026.017

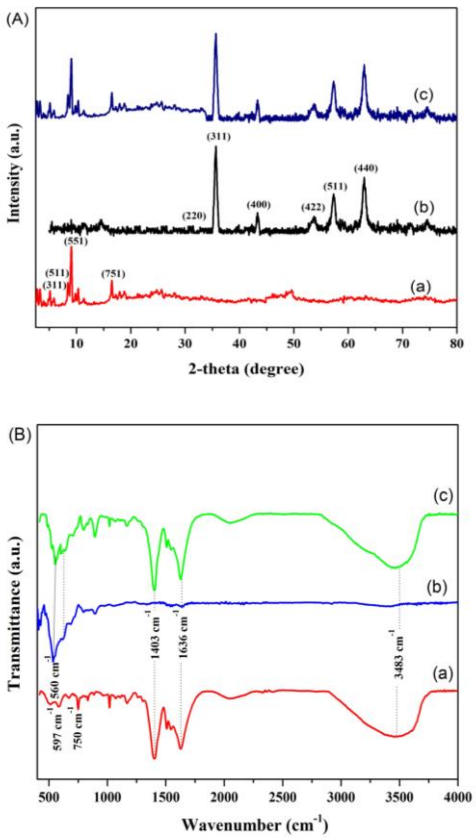

Fig. 1: (A) X-ray diffraction patterns, and (B) FT-IR of (a) MIL-101(Cr), (b) Fe_3O_4, and (c) Fe_3O_4@MIL-101(Cr) samples.

The FT-IR spectrum of Fe_3O_4@MIL-101(Cr) shows characteristic bands at around 1580–1620 and 1390–1410 cm^{-1} corresponding to the asymmetric and symmetric stretching vibrations of the carboxylate groups (COO^-) from the terephthalate ligand. A band at approximately 580 cm^{-1} is attributed to the Fe–O stretching vibration of magnetite. After the adsorption of polystyrene microplastics (Figure 5(d)), additional peaks were observed at approximately 3025, 2920, 1490, 756, and 698 cm^{-1}, corresponding to the characteristic vibrational modes of aromatic C–H bonds and the benzene ring of polystyrene. In addition, the SEM image (inset) obtained after adsorption reveals the presence of PS fibers attached to the surface of the material, further confirming the successful interaction between PS microplastics and the Fe_3O_4@MIL-101(Cr) composite.

The SEM images (Figure 2(a)) show that MIL-101(Cr) crystals exhibit a well-defined polyhedral morphology with relatively smooth surfaces. The particle size is mainly distributed in the range of several hundred nanometers, which is consistent with the typical morphology reported for MIL-101(Cr). The Fe_3O_4 nanoparticles (Figure 2(b)) exhibit a quasi-spherical morphology with particle sizes in the nanometer range. Due to the strong magnetic interaction, the nanoparticles tend to aggregate and form irregular clusters. After loading Fe_3O_4 nanoparticles (Figure 2(c,d)), the morphology of MIL-101(Cr) becomes rougher and numerous spherical nanoparticles are observed on the surface of the MOF crystals. These nanoparticles are uniformly distributed and form small clusters, indicating that Fe_3O_4 nanoparticles are successfully anchored onto the MIL-101(Cr) framework.

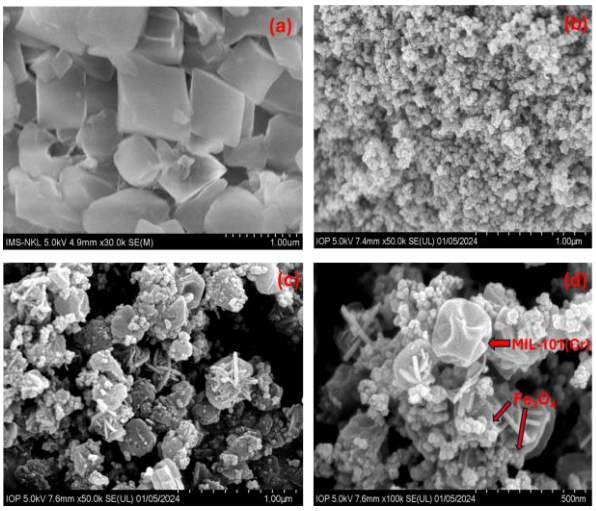

Fig. 2: SEM of (a) MIL-101(Cr), (b) Fe_3O_4, and (c,d) Fe_3O_4@MIL-101(Cr) samples.

The EDX profile (Figure 3) reveals the presence of C, O, Cr, and Fe elements, confirming the successful formation of the composite structure. The strong signals of carbon and oxygen observed at low energy regions are mainly attributed to the organic linker of the MIL-101(Cr) framework, which contains aromatic dicarboxylate ligands. The coexistence of Cr and Fe peaks demonstrates that the magnetic Fe-containing phase was successfully integrated with the MIL-101(Cr) matrix.

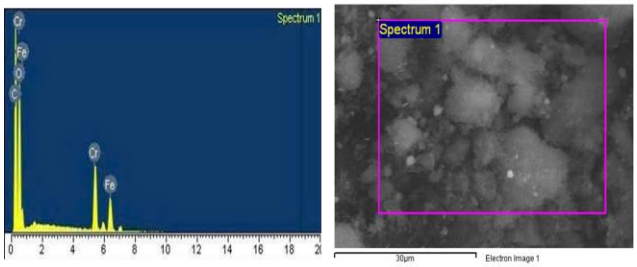

Fig. 3: EDX of Fe_3O_4@MIL-101(Cr) composite.

In this study, a 0.1 M KCl solution was used as the background electrolyte to determine the point of zero charge of the Fe_3O_4@MIL-101(Cr) composite. The

https://doi.org/10.62239/jca.2026.017

relationship between ΔpH and the initial pH (pH_i) of the suspension is presented in Figure 4. As shown in Figure 4(A), the point of zero charge (pH_pzc) of the Fe_3O_4@MIL-101(Cr) composite was determined to be 8.15. This result indicates that the surface of the composite exhibits a slightly alkaline character.

The pH at the point of zero charge (pH_pzc) of the Fe_3O_4@MIL-101(Cr) composite was determined from the pH_pzc plot, which shows a value of approximately 8.15, indicating that the surface of the material is electrically neutral at this pH. When pH < 8.15, the composite surface tends to be positively charged due to the protonation of hydroxyl groups (–OH) on the Fe_3O_4 surface as well as functional groups within the MIL-101(Cr) framework. In contrast, when pH > 8.15, the surface becomes negatively charged as a result of deprotonation processes.

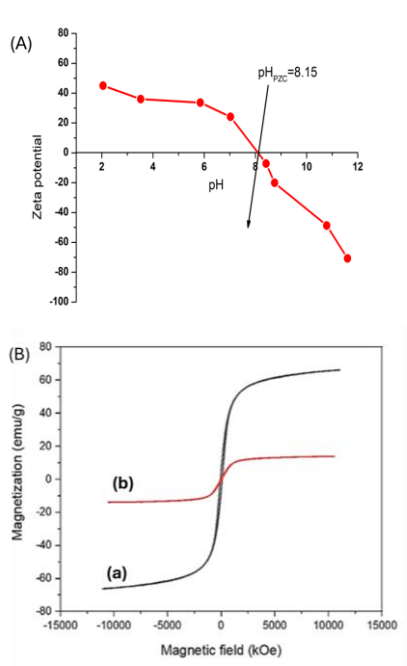

Fig. 4: (A) Point of zero charge determination of Fe_3O_4@MIL-101(Cr) composite, and (B) Magnetic hysteresis of (a) Fe_3O_4 and (b) Fe_3O_4@MIL-101(Cr) composite.

The magnetic behavior of the Fe_3O_4 nanoparticles and the synthesized Fe_3O_4@MIL-101(Cr) composite was investigated using a vibrating sample magnetometer (VSM) at room temperature. As shown in Figure 3(b), the magnetization curve of the Fe_3O_4 nanoparticles exhibits negligible coercivity (Hc ≈ 0 Oe) and remanent magnetization (Mr ≈ 0 emu g^{-1}), indicating typical superparamagnetic behavior with a measured saturation magnetization (Ms) of approximately 50 emu g^{-1}.

In contrast, the measured saturation magnetization of the Fe_3O_4@MIL-101(Cr) composite significantly decreased to about 18 emu g^{-1}. This reduction in Ms can be attributed to surface spin disorder, surface oxidation, or finite-size effects that commonly occur in magnetic nanoparticles after being incorporated into the porous MIL-101(Cr) framework [18]. Nevertheless, the composite still retains sufficient magnetic properties, enabling efficient magnetic separation and recovery of the material after the adsorption process.

Removal performance of PS microplastics

As shown in Figure 5(a), the adsorption of PS microplastics onto Fe_3O_4 nanoparticles proceeded rapidly during the initial stage (0–30 min), mainly due to the large number of available active sites on the nanoparticle surface. In the subsequent stage (30–120 min), the adsorption efficiency reached 74% and remained nearly constant with further increase in contact time.

This behavior suggests that the active sites gradually became saturated, leading to increased competition among PS molecules for the remaining adsorption sites and consequently limiting the adsorption rate. This trend may also be attributed to the large molecular size of PS, which restricts the deep penetration of PS molecules into the aggregated structures of the nanoparticles. In comparison, the adsorption efficiency reached a maximum of 77% for MIL-101(Cr) and 91.4% for the Fe_3O_4@MIL-101(Cr) composite after 150 min of contact time. The PS microplastics adsorption over Fe_3O_4@MIL-101(Cr) was evaluated through three repeated experiments, yielding an average value of 91.4 ± 3.74%. The RSD value of 4.09% indicates repeatability within the acceptable range of RSD < 5%.

Furthermore, as the PS concentration increased from 500 ppm to 700 ppm (Figure 5(b)), the adsorption efficiency decreased from 90% to 77%, respectively. This reduction may be attributed to particle–particle shielding effects among the adsorbate molecules, as well as the mutual coverage of nanoparticles, which limits the accessibility of active adsorption sites.

The effect of the Fe_3O_4@MIL-101(Cr) composite dosage (0.5, 0.75, 1.0, 1.25, and 1.5 g L^{-1}) on the adsorption efficiency of PS was also investigated at an initial PS concentration of 500 ppm, a temperature of 30 °C, and a contact time of 150 min. The results are presented in Figure 5(c). The adsorption efficiency increased from 67.2% to 85.1% as the composite dosage increased from 0.5 to 1.0 g L^{-1}, indicating that the initial surface area of the adsorbent was insufficient to capture all PS molecules present in the solution. When the adsorbent dosage was further increased to 1.25 g L^{-1}, the adsorption efficiency reached a

https://doi.org/10.62239/jca.2026.017

maximum value of 91.4%. This result is consistent with previous studies, where the adsorption of PS microplastics (PSMPs, 5 mg/L, 30 mL) by ZIF-67 achieved an efficiency of 92.1% [19], while the adsorption of PS on magnetic Fe_3O_4 nanomaterials exhibited a relatively lower efficiency (86.11 ± 6.21%) [20]. This improvement can be attributed to the increase in the total surface area and the corresponding rise in the number of accessible active sites on the nanoparticle surface, such as ─OH and ─$FeOH_2^+$ functional groups [21,22]. At this dosage (1.25 g L^{-1}), the amount of adsorbent was sufficient to capture nearly all PS molecules present in the solution. However, when the Fe_3O_4@MIL-101(Cr) dosage was further increased to 1.5 g L^{-1}, the adsorption efficiency decreased to 87.4%. This decline may be explained by the agglomeration of Fe_3O_4 nanoparticles at high concentrations within the composite matrix due to magnetic interactions or van der Waals forces, which reduces the effective surface area available for PS adsorption. Thus, hydrophobic interactions arise when the polymer chains of PS microplastics preferentially aggregate and adhere to the less polar surface regions of MIL-101(Cr), thereby minimizing their exposure to the aqueous environment. Concurrently, π–π interactions play a dominant role through the overlap between the π-electron system of the phenyl rings in PS and the conjugated π-system of the terephthalate ligands within the MIL-101(Cr) framework. These π–π interactions enhance the non-covalent attractive forces between the two phases, contributing to the stabilization of microplastic adsorption on the material surface. Owing to the synergistic effect of these mechanisms, MIL-101(Cr) exhibits an effective adsorption capacity toward PS microplastics. Therefore, a PS microplastic concentration of 500 ppm, an adsorbent dosage of 1.25 g L^{-1}, and pH = 8.15 were selected as the optimal conditions for the adsorption process using the Fe_3O_4@MIL-101(Cr) composite, and these conditions will be employed in subsequent investigations.

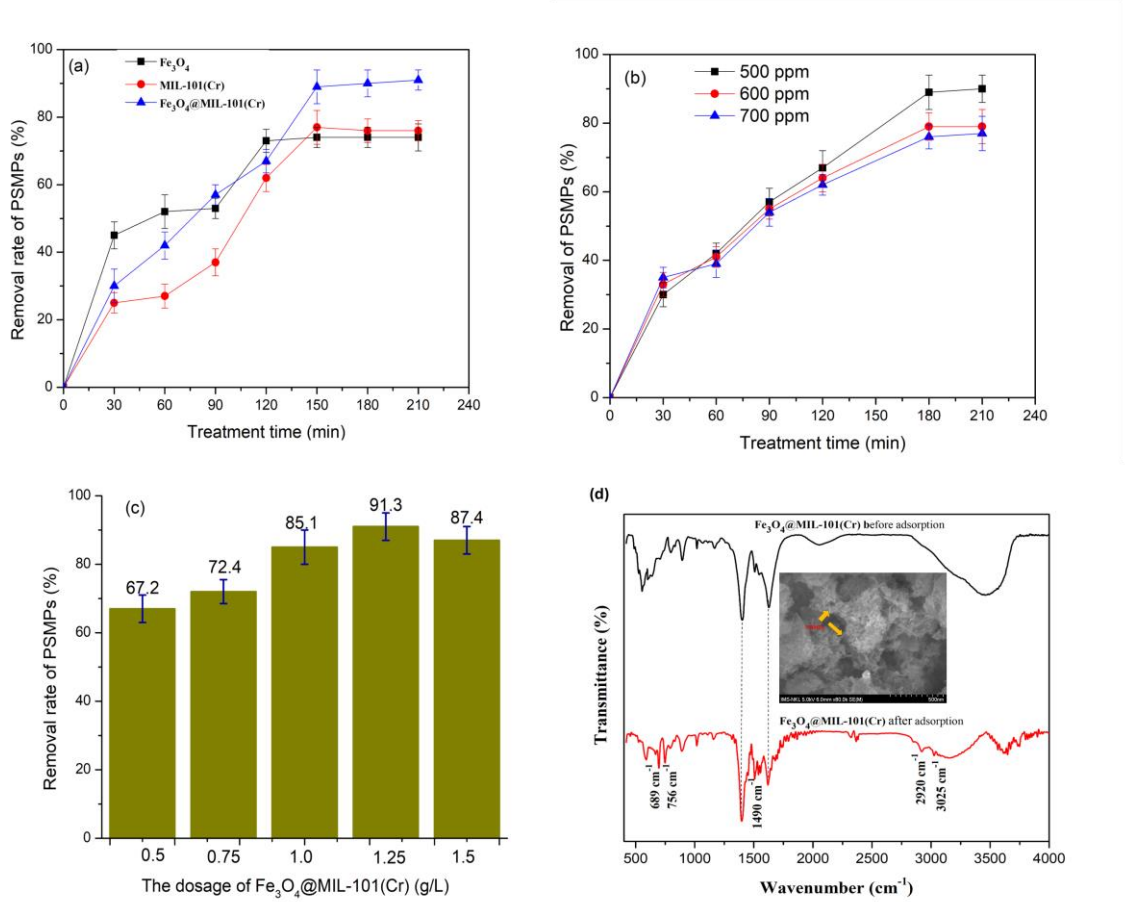

Fig. 5: Adsorption efficiency of PS microplastics: (a) on different materials (Fe_3O_4, MIL-101(Cr), and the Fe_3O_4@MIL-101(Cr) composite), (b) at different PS concentrations, (c) at different dosages of the Fe_3O_4@MIL-101(Cr) composite, and (d) FT-IR spectra of Fe_3O_4@MIL-101(Cr) before and after adsorption of PS microplastics (inset: SEM image of Fe_3O_4@MIL-101(Cr) after adsorption). Reaction conditions: room temperature, 30 °C; pH = 8.15; PS microplastic particle size = 500 nm.

https://doi.org/10.62239/jca.2026.017

Conclusion

The Fe_3O_4@MIL-101(Cr) composite was synthesized using an environmentally friendly approach with waste PET as the raw material source. Increasing the adsorbent dosage to 1.25 g L^{-1} and operating under mildly alkaline conditions (pH = 8.15) significantly enhanced the adsorption performance, achieving a PS microplastic removal efficiency of 91% within 150 min. These results further confirm the potential of magnetic nanocomposite materials for applications in water and wastewater treatment, particularly for the removal of organic pollutants, including microplastics, which have recently attracted significant environmental concern.

Acknowledgement

The authors gratefully acknowledge the financial support from the Ministry of Education and Training under the science and technology project (Grant No. B2024-MDA-10) for this research.

References

1. P. Holm, G. Schulz, K. Athanasopulu, Biol. Unserer Zeit, 43(1) (2013) 27–33. https://doi.org/10.1002/biuz.201310497
2. M. Darabi, M.R. Khosravi-Darani, A.A. Mohammadi, Springer, Cham (2021) 109–126. https://doi.org/10.1007/978-3-030-86879-7_5
3. S. Mishra, A.P. Das, Wastewater Treatment: Cutting-Edge Molecular Tools, Techniques and Applied Aspects, Elsevier (2021) 237–251. https://doi.org/10.1016/B978-0-12-821881-5.00011-8
4. D.K.A. Barnes, F. Galgani, R.C. Thompson, M. Barlaz, Philos. Trans. R. Soc. B Biol. Sci., 364(1526) (2009) 1985–1998. https://doi.org/10.1098/rstb.2008.0205
5. Y. Picó, D. Barceló, ACS Omega, 4(4) (2019) 6709–6719. https://doi.org/10.1021/acsomega.9b00222
6. K. Duis, A. Coors, Environ. Sci. Eur., 28 (2016) 1–25. https://doi.org/10.1186/s12302-016-0085-9
7. J. Barrett, A. Chase, C. Zhang, S. Hollands, P. Sutton, Front. Mar. Sci., 7 (2020) 576170. https://doi.org/10.3389/fmars.2020.576170
8. Y. Liu, W. Guo, X. Wang, S. Liu, Y. Liu, J. Hazard. Mater., 421 (2022) 126700. https://doi.org/10.1016/j.jhazmat.2021.126700
9. J. Ma, Y. Wang, J. Liu, H. Zhu, Y. Wang, Chemosphere, 307 (2022) 135749. https://doi.org/10.1016/j.chemosphere.2022.135749
10. M. Kaykhaii, M.R. Abolghasemi, R. Khosravi, A. Ebrahimi, Ind. Eng. Chem. Res., 62(9) (2023) 3835–3843. https://doi.org/10.1021/acs.iecr.2c04418
11. Y.-J. Chen, Y.-T. Li, J.-H. Kim, H.-S. Kim, D.-H. Kim, J. Mater. Chem. A, 8(29) (2020) 14644–14652. https://doi.org/10.1039/D0TA03829K
12. K.A. Adegoke, A. Alabi, O. Adebayo, S.A. Aderibigbe, Mar. Pollut. Bull., 187 (2023) 114546. https://doi.org/10.1016/j.marpolbul.2022.114546
13. G. Gnanasekaran, M. Saravanakumar, N.R. Babu, T. Arumugam, Sep. Purif. Technol., 277 (2021) 119655. https://doi.org/10.1016/j.seppur.2021.119655
14. A.A. Mohana, M. Yaseen Al-Gheethi, A. Al-Hashmi, A. Al-Khadhuri, Chemosphere, 309 (2022) 136682. https://doi.org/10.1016/j.chemosphere.2022.136682
15. X.N. Pham, V.-T. Vu, V.T.H. Nguyen, T.-T.-B. Nguyen, H.V. Doan, Nanoscale Adv., 4 (2022) 3600–3608. https://doi.org/10.1039/d2na00371f
16. V.T.H. Nguyen, T.T.-B. Nguyen, H.T. Nguyen, X.N. Pham, ChemNanoMat, 12 (2026) e202500677. https://doi.org/10.1002/cnma.202500677
17. X.-N. Pham, H.-H. Nguyen, H.T. Nguyen, T.T.-B. Nguyen, Chem. Eng. Technol., 48 (2026) e70135. https://doi.org/10.1002/ceat.70135
18. E. Bianchetti, C. Di Valentin, J. Phys. Chem. Lett., 13 (2022) 9348–9354. https://doi.org/10.1021/acs.jpclett.2c02186
19. H. Wan, J. Wang, X. Sheng, J. Yan, W. Zhang, Y. Xu, Toxics, 10 (2022) 70. https://doi.org/10.3390/toxics10020070
20. X. Shi, X. Zhang, W. Gao, Y. Zhang, D. He, Sci. Total Environ., 802 (2022) 149838. https://doi.org/10.1016/j.scitotenv.2021.149838
21. N. Singh, N. Khandelwal, Z.A. Ganie, E. Tiwari, G.K. Darbha, Chem. Eng. J., 418 (2021) 129405. https://doi.org/10.1016/j.cej.2021.129405
22. C. Shi, S. Zhang, J. Zhao, J. Ma, H. Wu, H. Sun, S. Cheng, Sep. Purif. Technol., 288 (2022) 120564. https://doi.org/10.1016/j.seppur.2022.120564